Article

Chinese Science Bulletin

Oceanology

June 2012 Vol.57 No.18: 2302–2306
doi: 10.1007/s11434-012-5137-8

Upper pycnocline turbulence in the northern South China Sea

LIU ZhiYu[1*] & LOZOVATSKY Iossif[2]

[1] *State Key Laboratory of Marine Environmental Science, College of Ocean and Earth Sciences, Xiamen University, Xiamen 361005, China;*
[2] *Environmental Fluid Dynamics Laboratories, Departments of Civil Engineering & Geological Sciences, University of Notre Dame, Notre Dame, IN 46556, USA*

Received October 12, 2011; accepted March 1, 2012; published online April 24, 2012

The first regional mapping of the averaged turbulent kinetic energy dissipation rate $<\varepsilon_p>$ in the upper pycnocline of the northern South China Sea is presented and discussed. At $\varphi = 20°$N and to the north of this latitude, $<\varepsilon_p>$ appears to be more than two times larger than that to the south of 20°N. It is suggested that this asymmetry is associated with the predominant northwestward propagation and dissipation of the internal waves originated in the Luzon Strait area. An approximately linear relationship between $<\varepsilon_p>$ and the available potential energy of the waves P_{IW}, suggests a characteristic time of the P_{IW} dissipation of about 6 h.

turbulence, internal waves, upper pycnocline, South China Sea

Citation: Liu Z Y, Lozovatsky I. Upper pycnocline turbulence in the northern South China Sea. Chin Sci Bull, 2012, 57: 2302–2306, doi: 10.1007/s11434-012-5137-8

The northern South China Sea (SCS) is featured by highly energetic internal tides (IT), which are predominantly generated in the region near the Luzon Strait (LS), and higher-frequency nonlinear internal waves (NLIW), which are among the strongest in the world's oceans [1]. Internal waves (IW) gradually evolve in the course of their northwestward propagation from LS crossing the deep central basin and steepening over the continental slope and shelf due to the shoaling effects. The IW energy dissipates mostly at the Dongsha Plateau and on a wide south-eastern shelf of China [2–4]. The importance of NLIW in turbulence generation, diapycnal mixing and submarine acoustics in the northern SCS has been explored by extensive measurements conducted during the Asian Sea International Acoustics Experiment [2,3,5] and the Nonlinear Internal Waves Initiative [1,6]. Based on these and other measurements, numerical modeling, and theoretical studies [7–11], our understanding of the processes responsible for wave generation, propagation and dissipation has been substantially elevated.

At the same time, there were almost no measurements of turbulence in the northern SCS until very recently. The turbulent kinetic energy (TKE) dissipation rate ε was indirectly estimated by Tian et al. [12] in the deep waters of SCS applying a semi-empirical formula of Gregg et al. [13] to LADCP and CTD data, and by Klymak et al. [6] and Alford et al. [14] using the Thorpe scale based approach [15] for CTD measurements. The first and the only direct measurements of micro scale shear (and therefore ε) in the northern SCS were conducted by St. Laurent [4] near the shelf break at the depth of 160 m. It was found that almost one third of the total dissipation in the water column occurred in a 10-m layer above the seafloor. The turbulence was presumably generated mostly by baroclinic motions rather than by regular bottom friction of barotropic tidal currents. No information is available about spatial variability of turbulence in the northern SCS, although it is of great importance for understanding and prediction of regional and global heat and momentum transports and various biogeochemical processes [12,16,17].

In this study, we attempt to shed light on the geography of turbulence in the upper pycnocline of the northern SCS, based on microstructure profiling measurements in the Luzon Strait, central deep basin, at the shelf break, and on the shelf. The spatial characteristics of ε are linked to the pre-

*Corresponding author (email: zyliu@xmu.edu.cn)

dominant northwestward propagation of IW originated in the LS region and dissipation of the wave energy.

1 Data

Microstructure measurements were conducted at 38 stations in the northern SCS during two cruises in the summer monsoon seasons of 2009 (July 25–August 13) and 2010 (May 17–21) using the MSS-60 profiler [18]. Twenty-four stations of the year 2009 cruise were mainly aligned along three cross-shelf sections marked in red in Figure 1 as E, A and S, respectively. In 2010, six stations were taken across LS and another eight stations located along two meridional sections, which were 30 and 60 miles to the west of LS (Figure 1, pink symbols, LS1–LS6 and O1–O8), respectively.

At each station, a series of 3 consecutive casts were launched during 10–20 min from the sea surface down to the bottom (at shallow stations) or to about 160 m depth in deep waters (limited by the length of a tethered cable of the profiler). The burst-averaged profiles of temperature T, salinity S, potential density σ_θ, and the TKE dissipation rate ε were obtained based on these data. The data processing followed a well-established procedure for the MSS measurements [19]. The accuracy of an individual estimate of ε is about 50% combining all kinds of errors [20]. The averaged over the upper pycnocline dissipation rate is supposed to be estimated with a higher accuracy.

2 Results

2.1 Mean dissipation rate in the upper pycnocline

Ocean turbulence is highly intermittent at small space and time scales (centimeters in all directions and minutes/seconds) as well as at mesoscales (a few meters/kilometers vertically/horizontally and hours). The later is usually referred as turbulence patchiness [21]. At the larger regional scales (tens or hundreds of kilometers and days/months), turbulence characteristics are expected to be linked to relatively stable larger-scale dynamical processes, which can be subjected to seasonal variability. Therefore, microstructure measurements conducted during the same seasons but in different years can be suitable to explore regional variability of turbulence in the northern SCS over tens and hundreds of kilometers.

We focused our analysis on spatial variations of the upper pycnocline ε in the SCS deep waters, and on the shelf between the surface mixed layer (SML) and the bottom boundary layer (BBL). The upper pycnocline turbulence is of particular biogeochemical importance because of the mixing induced cross-pycnocline transports of nutrients. This turbulence is assumed to be mostly influenced by IW of different scales. The averaged dissipation rate in the pycnocline under regular meteorological conditions is expected

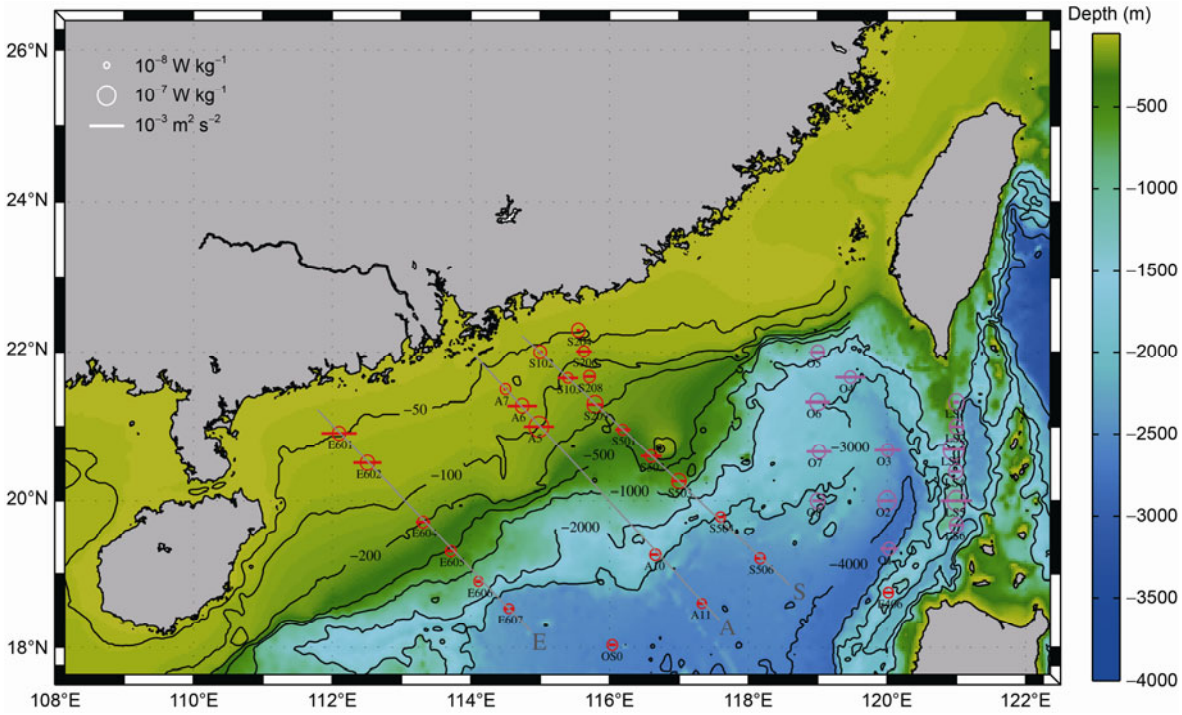

Figure 1 Stations of the 2009 (red) and 2010 (pink) cruises in the northern SCS. Three cross-shelf sections are marked as E, A and S. The spatial distributions of $<\varepsilon_p>$ and P_{IW} are shown by scaled circles (values are proportional to the areas of the circles) and scaled horizontal bars (values are proportional to the length of the bars), respectively.

to be relatively insensitive to the exact timing of measurements, and therefore can serve as a representative measure of turbulence at the measurement sites. On the contrary, turbulence in SML is mainly driven by variable atmospheric forcing. In BBL, it is mostly generated by bottom friction due to barotropic and/or baroclinic tidal flows timely dependent on tidal phases.

At the shelf stations, the pycnocline has been easily identified between SML and BBL, and the averaged dissipation rate $<\varepsilon_p>$ was calculated as

$$\left\langle \varepsilon_p \right\rangle = \frac{1}{h_{BBL} - h_{SML}} \int_{-h_{BBL}}^{-h_{SML}} \varepsilon(z)\mathrm{d}z, \tag{1a}$$

where h_{SML} and h_{BBL} are the lower boundary of SML and the upper boundary of BBL, respectively. The h_{SML} and h_{BBL} were estimated using the individual profiles of σ_θ and ε.

In deep waters, we selected the pycnocline segments immediately below SML, where density increases approximately linearly with depth, thus

$$\left\langle \varepsilon_p \right\rangle = \frac{1}{h_l - h_u} \int_{-h_l}^{-h_u} \varepsilon(z)\mathrm{d}z, \tag{1b}$$

where h_u and h_l are the depths of the upper and lower boundaries of the selected segments. The ε profiles were also employed in the selection procedure of h_u and h_l to make it more accurate.

Figure 2 shows the estimates $<\varepsilon_p>$ at all 38 stations. On the shelf, $<\varepsilon_p> = (3–6)\times10^{-8}$ W kg^{-1}, which is about 2–3 times lower than $<\varepsilon_p>$ near the shelf break, where it is elevated to 1.2×10^{-7} W kg^{-1}. It appears that 10 out of 12 of the deep-water ($H > 500$ m) stations taken in 2009 were located to the south of $\varphi = 20°$N. Only two stations (S502 and S503) were taken to the north of 20°N, but these are the stations with the highest level of $<\varepsilon_p> = (4.2 – 6.2)\times10^{-8}$ W kg^{-1}. These two stations are aligned almost directly to the west of the center of LS, where strong internal tidal waves are generated [1,22]. IW signatures in SAR images [23] and *in situ* measurements [24] showed that the IW fronts propagate mainly from LS toward west-northwest. If turbulence in the upper pycnocline is mostly associated with the degenerations of IW, it is expected to find a higher level of $<\varepsilon_p>$ in the northern part of SCS. In fact, for a joint set of 2009 and 2010 deep-water stations, the averaged dissipation rate in the upper pycnocline to the south of 20°N is $\overline{\left\langle \varepsilon_p \right\rangle}_{south} = 3.4\times10^{-8}$ W kg^{-1}, but it is more than two times larger at and to the north of 20°N, where $\overline{\left\langle \varepsilon_p \right\rangle}_{north} = 6.9\times10^{-8}$ W kg^{-1}. The maximum $<\varepsilon_p>_{max} = 1.3\times10^{-7}$ W kg^{-1} has been observed in the center of LS at station LS3 (Figures 1 and 2).

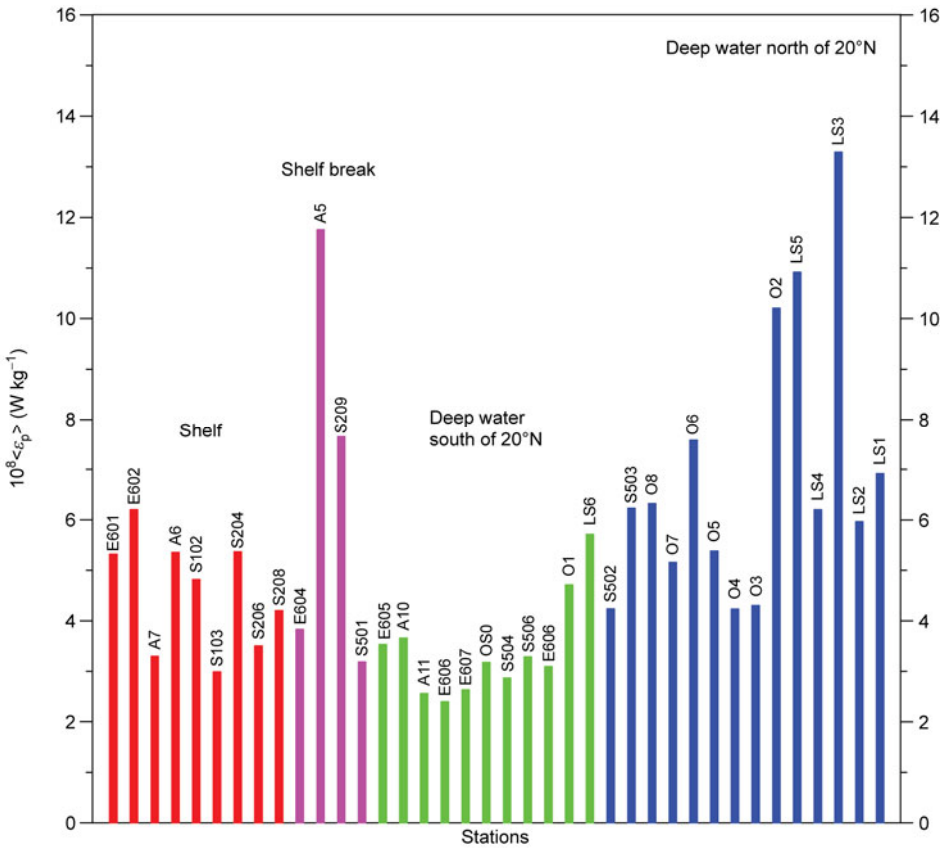

Figure 2 The averaged dissipation rate in the upper pycnocline $<\varepsilon_p>$ at all 38 stations (see also Figure 1).

2.2 Dissipation and APE of internal waves

We associate the disparity between $<\varepsilon_p>$ to the north and to the south of φ ~20°N with predominant propagation and degeneration of IW from the LS region, which is the main known source of IW in the northern SCS [1,2,22], to the west-northwest. To examine this assumption, we mapped $<\varepsilon_p>$ as the scaled circles in Figure 1 overlapping them by the scaled horizontal bars that represent the estimates of available potential energy (APE) of IW per unit mass, $P_{IW} = 1/2\,\eta_p^2 \left\langle N_p^2 \right\rangle$. Although the APE calculation is based on the linear theory of internal waves [25], it has been successfully used in many NLIW studies [26]. The wave displacements η_p were calculated as the rms of density disturbances $\rho'(z) = \rho(z) - \tilde{\rho}(z)$ divided by the mean density gradients in selected layers of the pycnocline [27]. Here $\tilde{\rho}(z)$ is the low-passed density profile filtered with a cutoff wavelength of 40 m. Although the results shown in Figure 1 do not point to a perfect match between the sizes of circles and bars, a general increasing trend of $<\varepsilon_p>$ with P_{IW} can be recognized specifically for the largest and smallest values of the mean dissipation.

To specify this trend, we plotted $<\varepsilon_p>$ against P_{IW} for each station as well as the bin-averaged (over 3 points) estimates of the dissipation rate and APE (Figure 3). It appears that $<\varepsilon_p>$ and P_{IW} are reasonably well correlated particularly for the bin-averaged samples. The coefficient of determination for the linear regression shown in Figure 3 is $r^2 = 0.7$. The regression can be specified in terms of a background dissipation rate ε_0, P_{IW}, and a characteristic time scale of the APE dissipation τ_{IW} as

$$<\varepsilon_p> = \varepsilon_0 + P_{IW}/\tau_{IW}, \quad (2)$$

where $\varepsilon_0 = 3.12\times10^{-8}$ W kg^{-1} and $\tau_{IW} \approx 5.8$ h. Eq. (2) suggests that the potential energy of IW in the pycnocline of the northern SCS dissipates during approximately 6 h increasing $<\varepsilon_p>$ proportionally to APE of IW. The background dissipation $\varepsilon_0 = 3.12\times10^{-8}$ W kg^{-1} is relatively high, which is possibly associated with a combined effect of the kinetic energy of IW as well as with turbulence generated by the shear instability of mean currents and other generation processes.

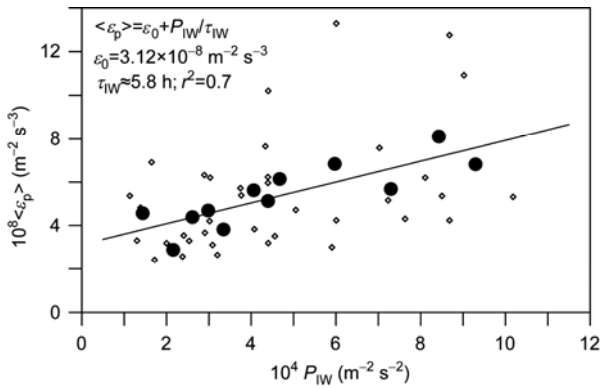

Figure 3 The averaged dissipation rate in the upper pycnocline $<\varepsilon_p>$ vs. the APE of internal waves P_{IW} at all 38 stations (open symbols) and the bin-averaged estimates (filled circles). Parameters of the linear regression are in the legend (see text for details). The 95% confidence limits for the estimates of $\varepsilon_0 = (1.84 - 4.12)\times10^{-8}$ W kg^{-1} and for $\tau_{IW} = 3.9 - 9.7$ h.

3 Summary and discussion

The first and the only microstructure measurements of turbulence in the northern SCS have been reported recently by St. Laurent [4] but for a very limited region near the shelf break to the north of Dongsha Plateau. The measurements reported here filled the observational gap spanning across the deep SCS basin from LS to the shallow shelf of China allowing to map the TKE dissipation $<\varepsilon_p>$ averaged over the upper pycnocline. Near the shelf break, $<\varepsilon_p>$ is elevated to ~ 1.2×10^{-7} W kg^{-1}; it is several times smaller on the shelf, where $<\varepsilon_p> = (3-6)\times10^{-8}$ W kg^{-1}, and it is almest an order of magnitude smaller in the upper pycnocline of the central deep basin. Substantial latitudinal asymmetry of $<\varepsilon_p>$ was found with respect to φ=20°N, which we linked to predominant northwestward propagation and dissipation of IW originated in the LS area. At and to the north of 20°N, $<\varepsilon_p>$ was more than two times larger than that to the south of this latitude. An approximately linear relationship between $<\varepsilon_p>$ and APE of IW P_{IW}, suggests a characteristic time of the P_{IW} dissipation of about 6 h.

Satellite images [28], *in situ* measurements [29], and numerical experiments [30] point to a substantial seasonal variability of IW activity in the northern SCS. Signatures of IW were most frequently observed in the summertime (70% of the annual IW signatures compare to only 1% during the winter). Spring and autumn account for 18% and 11% of the IW occurrence, respectively. This is mainly attributed to a much shallower and stronger summer pycnocline compared to the other seasons, which creates favorable conditions for IW generation and propagation. The upper pycnocline turbulence in the region, which is partially linked to the APE dissipation of IW, may also experience strong seasonal variability. Regional mapping of the upper pycnocline averaged dissipation reported here covers only the summer monsoon period. Further extensive microstructure measurements are needed to explore seasonal variability of turbulence in the northern SCS.

We are most grateful to Dr. Hao Wei for providing the MSS profiler for these measurements, which were funded by the State Key Laboratory of Marine Environmental Science (Xiamen University) and the National Basic Research Program of China (2009CB421200 and 2007CB411803). This work was supported by the National Natural Science Foundation of China (41006017 and 41076001), the Fundamental Research Funds for the Central Universities of China (2010121030), and the U.S. Office of Naval Research (N00014-05-1-0245).

1 Alford M H, Lien R C, Simmons H, et al. Speed and evolution of nonlinear internal waves transiting the South China Sea. J Phys Oceanogr, 2010, 40: 1338–1355
2 Lien R C, Tang T Y, Chang M H, et al. Energy of nonlinear internal waves in the South China Sea. Geophys Res Lett, 2005, 32: L05615
3 Chang M-H, Lien R C, Tang T Y, et al. Energy flux of nonlinear internal waves in northern South China Sea. Geophys Res Lett, 2006, 33: L03607
4 St. Laurent L. Turbulent dissipation on the margins of the South China Sea. Geophys Res Lett, 2008, 35: L23615
5 Duda T F, Lynch J F, Irish J D, et al. Internal tide and nonlinear internal wave behavior at the continental slope in the northern South China Sea. IEEE J Ocean Eng, 2004, 29: 1105–1130
6 Klymak J M, Alford M H, Pinkel R, et al. The breaking and scattering of the internal tide on a continental slope. J Phys Oceanogr, 2011, 41: 926–945
7 Fang W, Shi P, Long X, et al. Internal solitons in the northern South China Sea from *in situ* observations. Chin Sci Bull, 2005, 50: 1627–1631
8 Liang X, Zhang X, Tian J. Observation of internal tides and near-inertial motions in the upper 450 m layer of the northern South China Sea. Chin Sci Bull, 2005, 50: 2890–2895
9 Buijsman M C, Kanarska Y, McWilliams J C. On the generation and evolution of nonlinear internal waves in the South China Sea. J Geophys Res, 2010, 115: C02012
10 Cai S, Xie J. A propagation model for the internal solitary waves in the northern South China Sea. J Geophys Res, 2010, 115: C12074
11 Yuan Y, Zheng Q, Dai D, et al. Mechanism of internal waves in the Luzon Strait. J Geophys Res, 2006, 111: C11S17
12 Tian J, Yang Q, Zhao W. Enhanced diapycnal mixing in the South China Sea. J Phys Oceanogr, 2009, 39: 3191–3203
13 Gregg M C, Sanford T B, Winkel D P. Reduced mixing from the breaking of internal waves in equatorial ocean waters. Nature, 2003, 422: 513–515
14 Alford M H, MacKinnon J A, Nash J D, et al. Energy flux and dissipation in Luzon Strait: Two tales of two ridges. J Phys Oceanogr, 2011, 41: 2211–2222
15 Dillon T M. Vertical overturns: A comparison of Thorpe and Ozmidov length scales. J Geophys Res, 1982, 87: 9601–9613
16 Qu T, Girton J B, Whitehead J A. Deepwater overflow through Luzon Strait. J Geophys Res, 2006, 111: C01002
17 Dai M, Meng F, Tang T, et al. Excess total organic carbon in the intermediate water of the South China Sea and its export to the North Pacific. Geochem Geophys Geosyst, 2009, 10: Q12002
18 Prandke H, Stips A. Test measurements with an operational microstructure-turbulence profiler: Detection limits of dissipation rates. Aquat Sci, 1998, 60: 191–209
19 Liu Z, Wei H, Lozovatsky I D, et al. Late summer stratification, internal waves, and turbulence in the Yellow Sea. J Mar Syst, 2009, 77: 459–472
20 Lozovatsky I, Liu Z, Fernando H, et al. Shallow water tidal currents in close proximity to the seafloor and boundary-induced turbulence. Ocean Dynam, 2012, 62: 177–191
21 Lozovatsky I D, Roget E, Planella J, et al. Intermittency of near-bottom turbulence in tidal flow on a shallow shelf. J Geophys Res, 2010, 115: C05006
22 Jan S, Lien R C, Ting C H. Numerical study of baroclinic tides in Luzon Strait. J Oceanogr, 2008, 64: 789–802
23 Zhao Z, Klemas V, Zheng Q, et al. Remote sensing evidence for baroclinic tide origin of internal solitary waves in the northeastern South China Sea. Geophys Res Lett, 2004, 31: L06302
24 Ramp S R, Tang T Y, Duda T F, et al. Internal solitons in the northeastern South China Sea: Part I. Sources and deep water propagation. IEEE J Ocean Eng, 2004, 29: 1157–1181
25 Phillips O M. The Dynamics of the Upper Ocean. Cambridge: Cambridge University Press, 1977
26 Scotti A, Beardsley R, Butman B. On the interpretation of energy and energy fluxes of nonlinear internal waves: An example from Massachusetts Bay. J Fluid Mech, 2006, 561: 103–112
27 Lozovatsky I D, Morozov E G, Fernando H J S. Spatial decay of energy density of tidal internal waves. J Geophys Res, 2003, 108: 3201
28 Huang W, Johannessen J, Alpers W, et al. Spatial and temporal variations of internal waves in the northern South China Sea. In: 2nd Int. Workshop on advances in SAR oceanography from ENVISAT and ERC missions, 2008 Jan 21–25, Frascati, Italy
29 Ramp S R, Yang Y J, Bahr F L. Characterizing the nonlinear internal wave climate in the northeastern South China Sea. Nonlinear Process Geophys, 2010, 17: 481–498
30 Shaw P-T, Ko D S, Chao S-Y. Internal solitary waves induced by flow over a ridge: With applications to the northern South China Sea. J Geophys Res, 2009, 114: C02019